

Textile Research Journal

<http://trj.sagepub.com>

Influence of Slipping Friction on Stress Concentration in Blended Yarns

John N. Rossettos and Thomas A. Godfrey

Textile Research Journal 2005; 75; 43

DOI: 10.1177/004051750507500109

The online version of this article can be found at:

<http://trj.sagepub.com/cgi/content/abstract/75/1/43>

Published by:

 SAGE Publications

<http://www.sagepublications.com>

Additional services and information for *Textile Research Journal* can be found at:

Email Alerts: <http://trj.sagepub.com/cgi/alerts>

Subscriptions: <http://trj.sagepub.com/subscriptions>

Reprints: <http://www.sagepub.com/journalsReprints.nav>

Permissions: <http://www.sagepub.com/journalsPermissions.nav>

Influence of Slipping Friction on Stress Concentration in Blended Yarns

JOHN N. ROSSETTOS

*Department of Mechanical, Industrial & Manufacturing Engineering, Northeastern University,
Boston, Massachusetts 02115, U.S.A.*

THOMAS A. GODFREY

Natick Soldier Center, US Army Soldier & Biological Chemical Command Natick, Massachusetts 01760, U.S.A.

ABSTRACT

We report the effect of a variable frictional shear force distribution along a slipping broken fiber on the stress concentration (SCF) in blended yarns. Our micromechanical model leads to a system of second order differential equations, which we solve using a convenient eigenvector expansion approach. The results for an exponential variation of frictional shear on a slipping fiber, starting from zero at the broken end, are compared to those for a constant friction force. While the extent of the slip region increases by as much as 50% for the exponential variation compared to the constant friction case, the SCF changes only slightly, generally decreasing less than 6%. Decreases are smaller when a high elongation fiber is broken than when a low elongation fiber is broken. The hybrid effect in blended yarns, established in previous work, continues to be supported by these new results.

In studying damage growth (or the failure process) in yarns with fiber breaks, the magnitude of the slip friction that occurs near a broken slipping fiber plays an important role. It is certainly not clear how the magnitude of the friction force varies over the region where the broken fiber slips. In a previous study [9], we assumed the slip friction force was constant ("simple slip assumption") along the slip region, thereby simplifying the analysis. It would be of interest to ascertain how a frictional force that varies, starting from zero at the fiber break and increasing exponentially at different rates over the slip region, affects the results.

It is well known that blended yarns consisting of two or more different fibers have improved strength and stiffness compared to homogeneous yarns. We demonstrated this so-called hybrid effect analytically in earlier work [9] for yarns with two kinds of fibers, where we showed that the stress concentration factor (SCF) of an LE (low elongation) fiber next to a broken HE (high elongation) fiber decreases, while the SCF of an HE fiber next to a broken LE fiber increases with decreasing values of the hybrid parameter R , the ratio of the axial stiffness of the HE to that of the LE fibers. ($R = 1$ represents homogeneous yarns, and smaller fractional values of R indicate larger stiffness differences between the two fiber types.) The aforementioned results indicate a positive effect for yarns where the principal fibers are particular LE fibers

with dispersed HE fibers. We suggest that if the reduction of the SCF of the principal LE fiber has a dominant effect on the yarn strength compared with the increased SCF of the HE fiber (especially since the HE fiber has a larger failure strain), a hybrid effect can be realized.

Twisted fibrous structures such as yarns exhibit transverse compressive forces induced by the remote tension along the yarn axis. These forces permit load transfer to occur between abutting fibers through friction and give the yarn cohesiveness. With increasing yarn tension, transverse compressive forces also increase because of the quasi-helical path of each fiber through the yarn, thereby increasing the magnitude of frictional load transfer between fibers and the structural integrity of the yarn. Representative past work on yarn stress analysis by Hearle [3, pp. 175–212], Kilby [5], and Thwaites [10, 11] considered a helical element of the twisted yarn, with no attention given to broken fibers. However, the results for yarn internal stresses obtained in these studies have motivated our model of frictional load transfer at slipping fiber contact surfaces in the analytical treatment of broken fibers (Godfrey and Rossettos [2]). How such slipping friction, and its variation along the slip region, affects the SCF near a fiber break is an important objective of this work. The SCF has traditionally provided an indication of the load sharing by adjacent fibers next to fiber breaks. This information has been employed in the past to pre-

dict strength using the stochastic aspects of the failure process, from the early work of Daniels [1] to representative recent work by Phoenix [6], Pitt and Phoenix [7], and Realf *et al.* [8]. The work by Realf *et al.* [8] yielded important results for the failure of blended yarns.

The micromechanical model for a blended yarn, which we developed earlier [2] and used again [9] with some modification, will be modified again in this paper to treat a varying slip friction force along the slip region. The model consists of the same number LE and HE fibers undergoing axial extension, with a fiber break in the central region of the hybrid fiber array. The stress concentration in the fibers adjacent to the break will depend in an important way on whether the broken fiber is HE or LE. Note that our mathematical model has a mathematical structure similar to Hedgepeth and Van Dyke's [4] shear-lag model for a three-dimensional fiber composite, where the load transfer from the broken fiber to the adjacent intact fiber takes place by shear of the matrix. For packed fiber arrays in hybrid yarns, load transfer occurs through geometry changes in the fibers and surface friction

Analysis

We developed the fundamental differential equations of our model, together with the important deformation mechanisms, in reference [9]. For completeness, we will briefly include the basic development here, together with the modifications necessary for this new analysis. In our model of a twisted yarn, the fibers follow helical paths [3] and lie in co-axial concentric layers. In the central region of the yarn, the fibers are nearly parallel to the yarn axis, and they experience the highest strains during yarn extension. Since rupture usually starts in the central region, we base our model in this region. Near the yarn's center, the microstructure is represented by a square packed array of parallel fibers, where we assume roughly similar cross-sectional dimensions for HE and LE fibers [9].

We derive the equations of our model by considering an equal number of HE and LE fibers. A typical finite array is shown in Figure 1. The fibers are numbered (n, m) , where n is the column number and m is the row number. In Figure 1, the shaded fibers are LE and the blank fibers are HE. The center fiber $(0,0)$ in Figure 1 is an HE fiber and will be considered broken in the development to follow. The array is extended in the x -direction to a strain ϵ . The displacement reference is taken as the position of points on an undamaged fiber array under the same strain. The square region in Figure 1 exhibits eight-fold symmetry, and this will reduce the number of equations needed for the analysis.

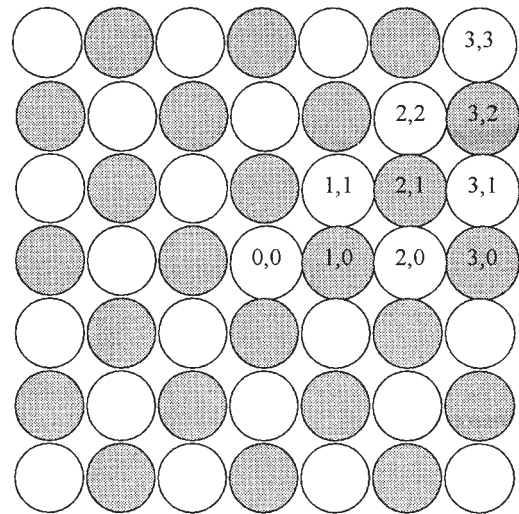


FIGURE 1. Numbering scheme for a finite section of a fiber array; LE fiber shown shaded.

The equilibrium equation for an (n, m) fiber in the case where there is no slip between fibers considers the shear forces (surface friction between fibers) acting on the (n, m) fiber from its four abutting fibers in Figure 2. The shear flow (shear force per unit length) is assumed [2] to be proportional to the difference in the displacement of the two abutting fibers. For instance, the shear flow $q_{n, n+1}^m$, caused by the $(n+1, m)$ fiber on the (n, m) th fiber, is taken as

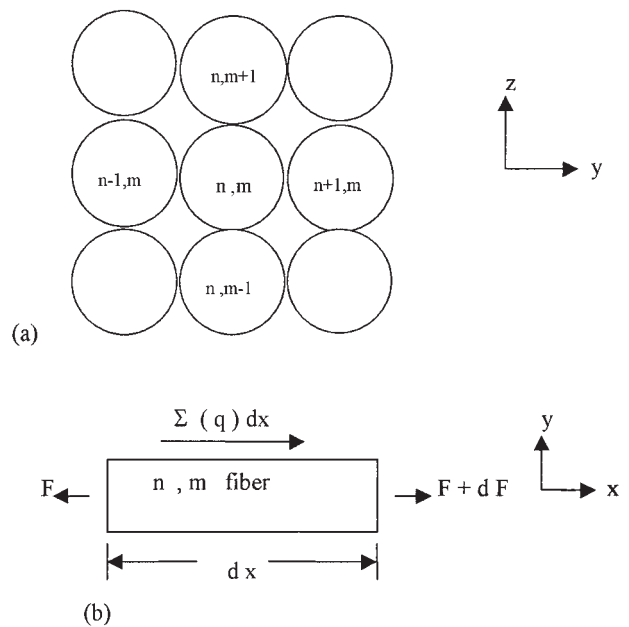


FIGURE 2. (a) n, m th fiber and abutters, (b) n, m th fiber equilibrium.

$$q_{n,n+1}^m = k(u_{n+1,m} - u_{n,m}) \quad (1)$$

The displacement pattern is taken so that the shear forces on the (n, m) fiber by the $(n + 1, m)$ and $(n, m + 1)$ fibers in Figure 2a are in the positive x -direction, while the forces on the (n, m) fiber by the $(n - 1, m)$ and $(n, m - 1)$ fibers are in the negative x -direction. E^*A^* and EA are the effective axial stiffness of the HE and LE fibers, respectively. Introduce $u_{n,m}$ as the axial (x -direction) displacement of fiber (n, m) at position x . If (n, m) is an HE fiber, then in Figure 2b, $dF = E^*A^*(d^2u_{n,m}/dx^2)dx$, so that equilibrium for fiber (n, m) can be written as

$$E^*A^* \frac{d^2u_{n,m}}{dx^2} + k(u_{n+1,m} - u_{n,m}) - k(u_{n,m} - u_{n-1,m}) + k(u_{n,m+1} - u_{n,m}) - k(u_{n,m} - u_{n,m-1}) = 0 \quad (2)$$

Nondimensional quantities, ξ and $U_{n,m}$ are defined by

$$x = \sqrt{E^*A^*/k} \xi, \quad u_{n,m} = \varepsilon \sqrt{E^*A^*/k} U_{n,m} \quad (3)$$

Equation 2 can then be written as

$$U_{n,m}'' + (U_{n+1,m} + U_{n-1,m} + U_{n,m+1} + U_{n,m-1} - 4U_{n,m}) = 0 \quad (4)$$

where primes denote differentiation with respect to ξ . It is instructive to write equations for fibers $(0,0)$, $(1,0)$ and $(1,1)$. Using Equation 4 to write the equation for fiber $(0,0)$ and noting the symmetry in Figure 1, where $U_{0,1} = U_{1,0} = U_{-1,0} = U_{0,-1}$, the equation can be written as

$$U_{0,0}'' + 4(U_{1,0} - U_{0,0}) = 0 \quad (5)$$

In a similar fashion, the equation for fiber $(1,1)$ can be obtained from Equation 4 by noting that $U_{1,2} = U_{2,1}$ and $U_{0,1} = U_{1,0}$, which gives

$$U_{1,1}'' + (2U_{2,1} + 2U_{1,0} - 4U_{1,1}) = 0 \quad (6)$$

Since fiber $(1,0)$ is an LE fiber its equation takes on a slightly different form than Equation 4. Its equilibrium equation (using $u_{1,-1} = u_{1,1}$ from symmetry) is given by

$$EA d^2u_{1,0}/dx^2 + ku_{2,0} - 4ku_{1,0} + k_{0,0} + 2ku_{1,1} = 0 \quad (7)$$

Using Equation 3, we can write Equation 7 in nondimensional form as

$$U_{1,0}'' + R(U_{2,0} + 2U_{1,1} + U_{0,0} - 4U_{1,0}) = 0 \quad (8)$$

where $R = E^*A^*/EA$. The parameter R is equal to 1 for nonhybrids and takes on fractional values in the range $1/6 \leq R \leq 1$ for blended (hybrid) yarns.

SLIP NEAR A FIBER BREAK

Assume slip occurs between the broken HE fiber and the abutting LE fibers (Figure 1), near the break, in the region $0 \leq x < a$. For the HE fiber $(0,0)$, equilibrium gives

$$E^*A^* d^2u_{0,0}/dx^2 - 4q_s g(\xi) = 0 \quad (9)$$

where q_s is a shear flow magnitude, so that $q_s g(\xi)$ is the shear/unit length along the contact line. The function $g(\xi)$ provides the variation of shear due to friction along the contact line and is given by

$$g(\xi) = (1 - e^{-\gamma\xi}) / (1 - e^{-\gamma\alpha}) \quad (10)$$

where α is the dimensionless slip region extent, so that $a = \sqrt{E^*A^*/k} \alpha$. The function $g(\xi)$ is plotted in Figure 3 for various values of the parameter $\gamma (=ga)$.

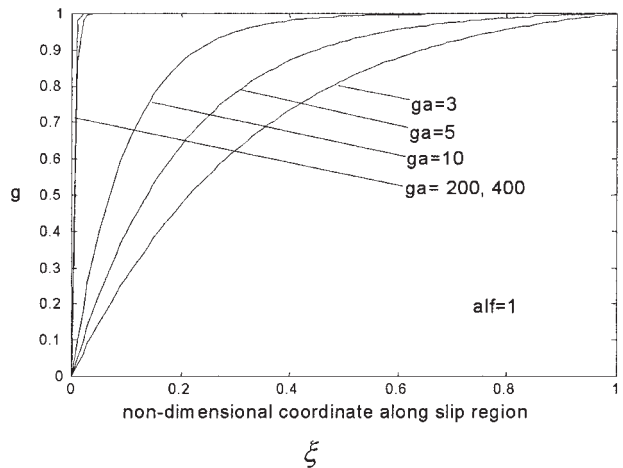


FIGURE 3. The function $g(\xi)$ versus ξ for various values of $\gamma (=ga)$; $\alpha = 1$.

If we define a shear parameter Q by $Q = q_s / \varepsilon \sqrt{kE^*A^*}$ and use Equation 3, Equation 9 becomes

$$U_{0,0}'' - 4Qg(\xi) = 0 \quad (11)$$

For the LE fiber $(1,0)$, slip occurs along the contact line with the HE fiber $(0,0)$, but there is no slip between it and the other three abutters. Writing the equilibrium equation and using symmetry, so that $U_{1,-1} = U_{1,1}$, the nondimensional equation can be derived as

$$U_{1,0}'' + R(U_{2,0} - 3U_{1,0} + 2U_{1,1}) + RQg(\xi) = 0 \quad (12)$$

For the HE fiber $(1,1)$ there are no slip surfaces, so equilibrium gives an equation identical to Equation 6.

We developed an expression for the shear flow magnitude, q_s in our earlier work [9]. We considered various

factors, including the lateral “hydrostatic” stress experienced by the fiber, the yarn surface helix angle, the axial strain, and the coefficient of friction between slipping fiber surfaces. Since q_s is expected to increase with strain, leveling off as the yarn approaches a taut condition, the shear flow is given by $q_s = \mu_0 d \bar{E} \varepsilon^{1-n} \eta$, where \bar{E} is the axial stiffness of the fiber array, d is the average fiber spacing, μ_0 is a constant and η is a function of the yarn helix angle. The friction index n can take on fractional values. We use values of n ranging from 0.5 to 0.9 in these results. Next we define a nondimensional shear flow by $\bar{q}_s = q_s / \mu_0 d \bar{E} \eta$. When plotted against strain ε , the quantity, \bar{q}_s , as indicated in Figure 4, approaches (asymptotic) taut condition values more steeply when $n = 0.9$ than say, when $n = 0.5$. Values of n at the higher end, $n = 0.9$, represent stiffer yarns where tautness occurs at lower strains. Values of n at the lower end, $n = 0.5$, represent more flexible yarns.

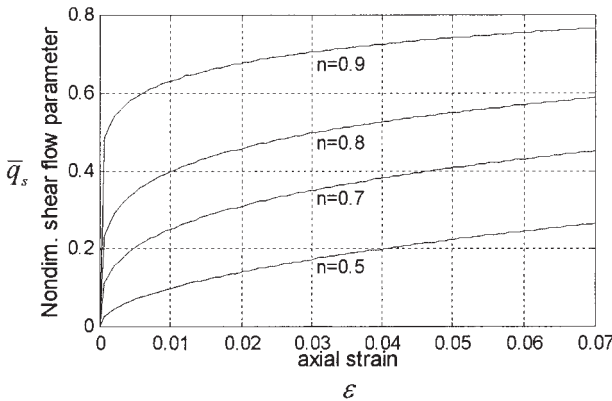


FIGURE 4. Shear flow parameter \bar{q}_s versus axial strain ε for various values of friction index n .

NONDIMENSIONAL FIBER LOADS

We denote by $p_{n,m}$ and $p_{n,m}^*$ the changes in loads in the LE and HE fibers, respectively, due to a fiber break. Far from the break, these loads are denoted by p and p^* , respectively. Dimensionless loads $P_{n,m}$ and $P_{n,m}^*$ are then defined by $(p_{n,m}, p_{n,m}^*) = p^* (P_{n,m}, P_{n,m}^*)$.

We assume a uniform strain far from the break, so that the strain there can be written as $\varepsilon = p^* / E^* A^* = p / EA$. The total load in, say, the HE fiber adjacent to the break is then given by $p^* + p_{n,m}^*$, where p^* is the reference load before the break. Noting that $p_{n,m}^* = E^* A^* du_{n,m}^* / dx$, and using Equations 3 and the definition of dimensionless loads, the total nondimensional load for the HE fiber can be written as $P_{n,m}^* = 1 + U_{n,m}'$. Note that, by definition, $P_{n,m}^* = p_{n,m}^* / p^*$ is in fact, the stress

concentration factor (SCF). With the expression for $q_s = \mu_0 d \bar{E} \varepsilon^{1-n} \eta$ and noting that the strain $\varepsilon = p / EA$, the shear parameter Q , can be written as

$$Q = \frac{\mu_0 d \bar{E} \eta (EA)^n}{p^n \sqrt{k E^* A^*}} \tag{13}$$

BOUNDARY VALUE PROBLEM

Because of the eight-fold symmetry, we need only write equations in a right triangular wedge, where the rows and columns number from 0 to M ($M = 3$ in Figure 1). It turns out that choosing $M = 2$ or 4 makes a negligible difference in the results, indicating that the significant deformations occur near the broken fiber.

Although we derived the equations here for only the center HE fiber (0,0) and its neighboring fibers (Equations 5, 6, 8, 11, 12), the equations for a larger wedge ($M = 3, 4, \dots$) can be developed in a similar and straightforward manner. In general, we will be dealing with a system of second-order differential equations. For illustrative purposes, the solution procedure will be described for the small wedge consisting of fibers (0,0), (1,0), and (1,1). The associated square region consists of nine fibers, and the influence of fibers outside the square is neglected. The eigenvector expansion technique used here is very convenient for larger systems such as six-fiber or greater wedges.

Slip will occur between the broken HE fiber (0,0) and its LE abutters (Figure 1) in a region $0 \leq x < a$, where a is the extent of the slip region. The corresponding dimensionless slip region extent is denoted by α , where $a = \sqrt{E^* A^*} / k \alpha$ using Equation 3. The unit cell is divided into region I, $0 \leq \xi < \alpha$, where slip occurs, and region II, $\alpha \leq \xi$, where no slip occurs. The system of equations in the nonslip region II consists of Equations 5, 6, and 8. In the eigenvector expansion technique, the equations are written in matrix form as

$$d^2 \mathbf{U} / d\xi^2 - \mathbf{A} \mathbf{U} = \mathbf{0}, \mathbf{U}^T = [U_{0,0} \quad U_{1,0} \quad U_{1,1}] \tag{14}$$

where \mathbf{A} is an appropriate matrix consistent with the solution vector \mathbf{U} . Since the equations have constant coefficients, a solution is assumed in the form $\mathbf{U} = \mathbf{R} e^{\lambda \xi}$, where \mathbf{R} is of the same order as \mathbf{U} . Substituting into Equation 14 gives $\mathbf{A} \mathbf{R} = \lambda^2 \mathbf{R}$. Using MATLAB, eigenvalues l_1, l_2, l_3 ($l_i = \sqrt{\lambda_i^2}$) and corresponding eigenvectors $\mathbf{r}_1, \mathbf{r}_2, \mathbf{r}_3$ are easily obtained. The solution is then given by

$$\mathbf{U} = \sum_{i=1}^3 c_i \mathbf{r}_i e^{-l_i \xi} \tag{15}$$

where positive exponents are dropped for bounded solutions in region II as $\xi \rightarrow \infty$. The constants of integration c_i are determined using appropriate continuity conditions.

In region I (slip region), Equations 11, 12, and 6 apply. Since Equation 11 is decoupled from the others, it can be integrated directly. The other equations need to be solved simultaneously and include particular solutions that are functions of ξ , often providing a challenge. The homogeneous equations are easily solved using the eigenvector expansion, and they include both positive and negative exponentials. The boundary conditions at $x = 0$ apply to solutions in region I. Since fiber (0,0) is stress-free (broken) so that $P_{0,0}^* = 0$, the equation $P_{n,m}^* = 1 + U_{n,m}'$ for the load gives $U_{0,0}' = -1$. For the intact fibers at $\xi = 0$, symmetry gives $U_{n,m}(0) = 0$, $(n, m) \neq (0,0)$. The solutions in the slip region for the small wedge ($M = 2$), which satisfy these boundary conditions, can be written as

$$U_{0,0} = \frac{2Q}{d} \xi^2 - \left(1 + \frac{4Q}{\gamma d}\right) \xi + A_0 - \frac{4Q}{\gamma^2 d} e^{-\gamma \xi} \quad (16)$$

For the remaining equations, the k th component of the U vector ($U_1 = U_{1,0}$; $U_2 = U_{1,1}$) is

$$U_k = -\sum_{i=1}^2 2A_i r_k^i \sinh(l_i \xi) + (Q/d) \sum_{i=1}^2 r_k^i f_i e^{l_i \xi} + U_{pk} \quad (17)$$

The particular solution components are $U_{p1} = (Q/2d)(1 + f_3 e^{-\gamma \xi})$, $U_{p2} = (Q/4d)(1 + f_4 e^{-\gamma \xi})$, and $d = 1 - e^{-\gamma \alpha}$. The quantities f_i ($i = 1, \dots, 4$) are given in terms of γ , R , and appropriate components of the eigenvectors \mathbf{r}^i (l_i are corresponding eigenvalues) in the slip region. The constants of integration A_0, A_1, A_2 and the quantity Q also need to be determined by requiring continuity between regions I and II at $\xi = \alpha$, where fibers are continuous. The following continuity conditions hold; $U_{n,m}^I(\alpha) = U_{n,m}^{II}(\alpha)$, $U_{n,m}'^I(\alpha) = U_{n,m}'^{II}(\alpha)$. An additional condition arises from the assumption that slipping is approached in a continuous manner—the shear flows on the broken fiber in the nonslipping region approach those in the slipping region as $\xi \rightarrow \alpha$. Using Equations 5 and 11, this condition may be written as $Q = [U_{0,0}^{II}(\alpha) - U_{1,0}^{II}(\alpha)]$.

The solution process proceeds by selecting values of the slip region extent α (this defines the two regions), and then determining the values of the integration constants and parameter Q such that the continuity conditions are satisfied. Results for the stress concentration factor (SCF) and slip extent will be plotted against the parameter p/p_L , where p_L is the applied load far from the break, which

just starts slipping, and p is the corresponding current load above that value. The ratio p/p_L can be obtained from Equation 13, where Q is proportional to $1/p^n$ for fixed material and geometric properties. Therefore, we get $p/p_L = (Q_L/Q)^{1/n}$, where Q_L is the corresponding value of Q when slipping just begins. Since the values of Q_L and Q are obtained as part of the solution process, p/p_L can be calculated.

Results and Discussion

The equations in the text have been developed for a broken center HE fiber. To obtain results for a broken LE fiber, the equations are modified as follows. An R (hybrid parameter) is placed in front of the parentheses in Equations 5 and 6, and is removed from Equation 7. Also, an R is placed before the Q term in Equation 12 and removed completely (two places) from Equation 13.

The nondimensional slip extent α is plotted against p/p_L in Figure 5 for various values of γ ($= ga$) for the case where an LE fiber is broken. Recall that values of γ determine the degree of frictional variation in the slip region (see Equation 10). Note also that p_L is the remote (far from the break) fiber load, which just initiates slipping, while p is the current load value above p_L . Curves are given for a fixed value of the hybrid parameter, R and for a value of $n = 0.8$. As shown in Figure 3, the curve for $\gamma = 200$ depicts an essentially constant friction along the slip region. In Figure 5, an increase in slip extent of about 50% is indicated over the range of p/p_L as values of γ decrease from 200 to 3. The smaller value of γ represents less friction, hence the larger slip extent. It also turns out that for a value of spring index $n = 0.5$ (not

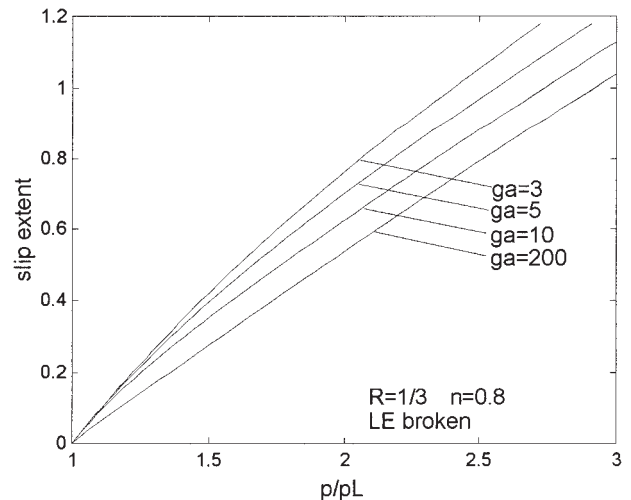


FIGURE 5. Slip extent α versus p/p_L ; LE fiber is broken, $n = 0.8$.

shown) and a fixed value of $\gamma = 3$, there is a 30% decrease in slip extent compared to that for $n = 0.8$. These changes are much less severe for stress concentration (SCF). In Figure 6, the SCF in the intact fiber adjacent to the broken fiber is plotted against p/p_L for the same conditions as in Figure 5. The SCF is less than 6% different between the curves for $\gamma = 200$ and $\gamma = 3$ and is smaller for $\gamma = 3$. Also, the SCF is only 2.5% higher for $n = 0.5$ as compared to $n = 0.8$ for $\gamma = 3$.

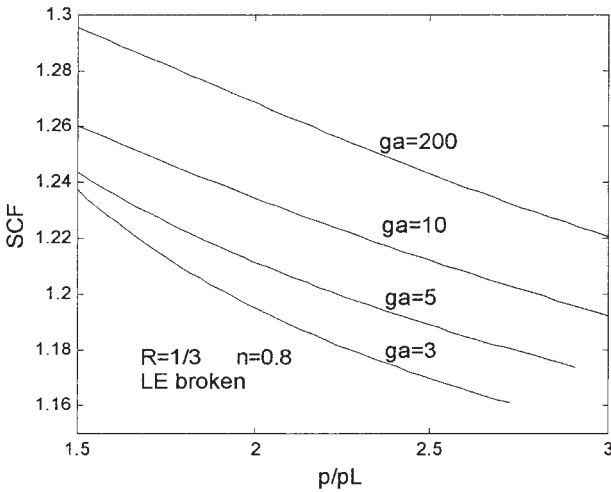


FIGURE 6. Stress concentration factor (SCF) versus p/p_L ; LE fiber is broken, $n = 0.8$.

In Figures 7 and 8, all conditions are the same as for Figures 5 and 6, except that now the broken fiber is an HE fiber. A 50% increase in slip extent is again observed in Figure 7 as γ goes from 200 to 3. When $n = 0.5$ (not shown), we get a 40% smaller slip extent than for $n = 0.8$, for $\gamma = 3$. Figure 8 shows that when an HE fiber is broken, the results are very different from when an LE fiber is broken. First, the level of SCF is very small, and the changes as γ goes from 3 to 200 are less than 1%. Also the $n = 0.5$ case shows negligible change. It appears that the higher load carried by the stiffer fiber (LE fiber) for a given strain level is partly transferred, when it breaks, to the adjacent fiber, thereby yielding the higher SCF shown in Figure 6. Note, also, the fact that the SCF decreases as the friction index n increases which can be explained by observing that for a given axial strain ϵ , the shear flow \bar{q}_s will increase with n as shown in Figure 4. This implies that for a larger n , a given slip region, with the larger shear (friction) forces developed, will take on more of the load of the broken fiber and hence lead to a smaller SCF. We can also interpret this as more energy being dissipated in the slip region.

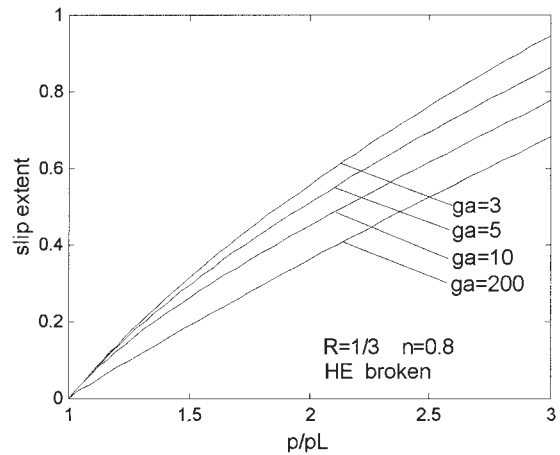


FIGURE 7. Slip extent α versus p/p_L ; HE fiber is broken, $n = 0.8$.

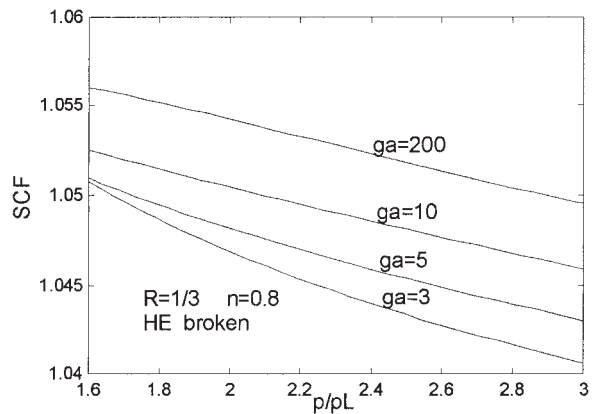


FIGURE 8. Stress concentration factor (SCF) versus p/p_L ; HE fiber is broken, $n = 0.8$.

In Figure 9, the SCF is plotted against the hybrid parameter R for various values of γ . The load level is selected as $p/p_L = 2$, and the separate cases of HE and LE broken fibers are both shown. The sensitivity of SCF to R is clearly indicated, with a more sharply increasing SCF for the case where an LE fiber is broken, and a mildly decreasing SCF in the case where an HE fiber is broken. As we can see, this trend is established for the range of values of γ from 3 to 200, so that the choice of γ (frictional variability) does not alter the important effect of the hybrid parameter R . We also discussed this in our earlier work [9], indicating a beneficial hybrid effect in blended yarns.

Conclusions

We have studied the effect of frictional shear along slipping fibers near a fiber break for blended yarns,

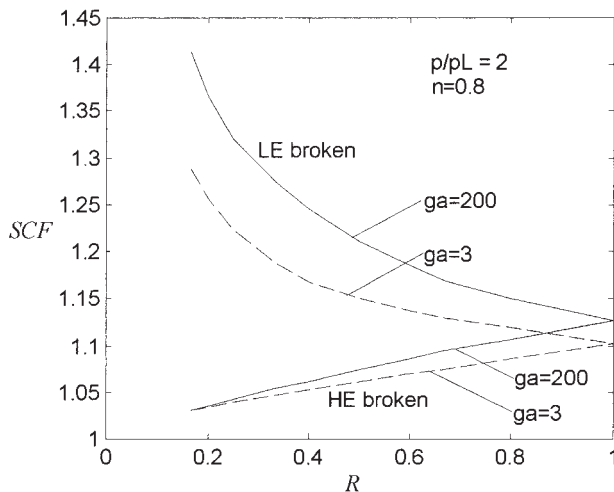


FIGURE 9. SCF versus R for various values of γ ($=ga$) for the separate cases of HE and LE broken fibers. Load level, $p/p_L = 2$.

consisting of an equal number of low elongation (LE) and high elongation (HE) fibers, undergoing axial extension. In general, the friction force on the slipping fiber is variable. In the model used here, it is taken to be zero at the cut end if the fiber has an exponential variation as it approaches a constant value with increasing distance from the break. The steepness of the approach to a constant value depends on a parameter γ . The slip region extent and the stress concentration (SCF) are determined for various values of γ and compared with the results, assuming constant friction (obtained for very large values of γ , such as $\gamma = 200$). In general, the smaller value of $\gamma = 3$ gives about a 50% increase in slip region extent compared to $\gamma = 200$ for a range of load levels. The SCF, however, shows differences of less than 6% between $\gamma = 200$ and $\gamma = 3$, and is smaller for $\gamma = 3$. The differences are greater when an LE fiber is broken than when an HE fiber is broken. The hybrid effect, pointed

out in reference [9], continues to be supported by the results given here for variable slipping friction near the fiber break.

Literature Cited

1. Daniels, H. E., The Statistical Theory of Strength of Bundles of Threads, *Proc. R. Soc. London A* **183**, 405–435 (1945).
2. Godfrey, T. A., and Rossettos, J. N., A Constitutive Model for the Extension of Blended Yarns with Fragmented Low-Elongation Fibers, *Textile Res. J.* **71**, 845–854 (2001).
3. Hearle, J. W. S., Grosberg, P., and Backer, S., “Structural Mechanics of Fibers, Yarns, and Fabrics,” Wiley-Interscience, NY, 1969.
4. Hedgepeth, J. M., and Van Dyke, P., Local Stress Concentrations in Imperfect Filamentary Composite Materials, *J. Compos. Mater.* **1**, 294–309 (1967).
5. Kilby, W. F., The Mechanical Properties of Twisted Continuous-Filament Yarns, *J. Textile Inst.* **55**, T589–T632 (1964).
6. Phoenix, S. L., Statistical Theory for the Strength of Twisted Fiber Bundles with Applications to Yarns, *Textile Res. J.* **49**, 407–423 (1979).
7. Pitt, R. E., and Phoenix, S. L., On Modelling the Statistical Strength of Yarns and Cables Under Localized Load-Sharing Among Fibers, *Textile Res. J.* **51**, 408–425 (1981).
8. Realff, M. L., Pan, N., Seo, M., Boyce, M. C., and Backer, S., A Stochastic Simulation of the Failure Process and Ultimate Strength of Blended Continuous Yarns, *Textile Res. J.* **70**(5), 415–430 (2000).
9. Rossettos, J. N., and Godfrey, T. A., Hybrid Effect at Fiber Breaks in Twisted Blended Yarns, *Textile Res. J.* **72**, 313–319 (2002).
10. Thwaites, J. J., The Elastic Deformation of a Rod with Helical Anisotropy, *Int. J. Mech. Sci.* **19**, 161–168 (1976).
11. Thwaites, J. J., “Mechanics of Flexible Fibre Assemblies,” Sijthoff & Noordhoff, Alphen aan den Rijn, The Netherlands, 1980, pp. 87–112

Manuscript received September 19, 2003; accepted January 13, 2004.